

Nonlinear enhancement of the dielectric properties of PVA-Al₂O₃ nanocomposites

Ram J. Sengwa*, Shobhna Choudhary

Dielectric Research Laboratory, Department of Physics, Jai Narain Vyas University, Jodhpur 342 005, India

*Corresponding author, E-mail: rjsengwa@rediffmail.com

Received: 27 March 2016, Revised: 12 September 2016 and Accepted: 21 September 2016

DOI: 10.5185/amp.2017/415
www.vbripress.com/amp

Abstract

Dielectric dispersion and relaxation behaviour of aqueous solution grown polymeric nanocomposite films consisting of poly(vinyl alcohol) (PVA) and alumina (Al₂O₃) (PVA-*x* wt% Al₂O₃ (*x* = 0, 1, 3 and 5)) have been studied in the frequency range from 20 Hz to 1 MHz by employing dielectric relaxation spectroscopy (DRS). It is found that at constant frequency, the real part of complex permittivity increases nonlinearly with the increase of Al₂O₃ nanoparticles concentrations in the PVA matrix, whereas it decreases with increase of frequency at constant concentration of Al₂O₃. The temperature dependent investigation on PVA-3 wt% Al₂O₃ film reveals that the dielectric properties increase with the increase of temperature confirming its thermally activated dielectric behaviour. The ac electrical conductivity of the nanocomposites increases and the impedance values decreases with the increase of frequency which are moderately affected by Al₂O₃ concentrations (*x* = 0 to 5 wt%) and temperatures (30 to 60 °C). The dc conductivity and relaxation time of PVA chain segmental motion of the nanocomposites obey the Arrhenius behaviour. The X-ray diffraction (XRD) study reveals that the crystallite size and amorphous phase of PVA increase with the increase of Al₂O₃ concentration in the PVA-Al₂O₃ nanocomposites. Results of this study confirm the suitability of PVA-Al₂O₃ nanocomposite materials as tunable nanodielectric for their use as insulator and substrate in the fabrication of microelectronic devices operated at audio and radio frequencies. Copyright © 2017 VBRI Press.

Keywords: Polymer nanocomposites, dielectric properties, electrical conductivity, polymer dynamics, X-ray diffraction.

Introduction

Polymer matrix dispersed with inorganic nanofiller by a state-of-the-art process resulted in the polymeric nanocomposites (PNCs) [1–4]. These are technologically advanced materials because of bearing the combine useful properties of both the polymer as well as nanofiller. Characterizations of thermal, mechanical, electrical, optical, magnetic and structural properties of such flexible-type novel PNC materials have been subject of intense research [1–11].

The investigations on alumina (aluminum oxide) (Al₂O₃) nanoparticles dispersed in poly(vinyl alcohol) (PVA) matrix based PNCs have realized tremendous improvement in their useful properties [12–19]. The Al₂O₃ nanoparticles have excellent characteristics including high adsorption capacity, wear resistance, thermal stability, electrical insulation, good thermal conductivity, high strength and stiffness, better mechanical strength, inertness to most of the acids and alkalis, and also non-toxic and inexpensive [20]. Further, Al₂O₃ exhibits numerous metastable crystalline phases through thermal transformation and such alumina are called transition aluminas denoted by γ -, δ -, α -, θ -Al₂O₃, etc. Among these phases of Al₂O₃ the thermodynamically

stable phase is α -Al₂O₃ which is obtained by appropriate thermal treatment above 1200 °C [21–24]. The γ -Al₂O₃ is a long known important catalyst which has been used in various chemical processes [25].

PVA is a polar, hydrophilic, non-toxic, biocompatible and hot water soluble semicrystalline polymer. In aqueous solution, the interaction between hydroxyl (–OH) groups of PVA chain and the oxygen atoms present on alumina nanoparticle surface turned the material into nanocomposite form. The interfacial interaction between PVA chain and Al₂O₃ nanoparticles also influences the PVA chain mobility in the interfacial region which is the most decisive factor governing the various properties of PVA-Al₂O₃ nanocomposites.

Although, the thermophysical and structural properties of PVA-Al₂O₃ nanocomposites has already been explored [12–17], but their dielectric and electrical properties were less attempted [18,19]. Therefore, in this paper the detailed dielectric behaviour and polymer relaxation process of PVA-Al₂O₃ nanocomposites have been investigated by employing dielectric relaxation spectroscopy (DRS). The DRS is a powerful technique for the characterization of various dielectric and electrical properties, and also the structural dynamics of the PNC

materials [7–10]. The effect of γ -Al₂O₃ nanofiller on dielectric properties of the nanocomposites has been explored by comparative analysis of the complex permittivity and electric modulus spectra. Further, ac electrical conductivity and impedance behaviour of these nanocomposites have also been reported and discussed in order to explore their suitability as insulator and substrate materials in designing and fabrication of microelectronic devices [1,2].

Experimental

Material

PVA ($M_w = 77000 \text{ g mol}^{-1}$) of laboratory grade was purchased from Loba Chemie, India. The Al₂O₃ nanopowder of particles sizes less than 50 nm as determined by manufacturer using transmission electron microscopy (TEM) was obtained from Sigma-Aldrich, Austria.

The nanocomposites of PVA dispersed with x wt% amount of Al₂O₃ ($x = 0, 1, 3$ and 5 wt% amounts of Al₂O₃ to the weight of PVA amount) were prepared by solution casting method. For each sample, initially 1 g of PVA was dissolved in 20 ml double distilled deionized water through heating up to 90 °C. The required amount of Al₂O₃ for each sample was firstly dispersed in 10 ml water. After that the aqueous PVA solution was mixed with Al₂O₃ dispersed aqueous solution and the same was magnetically stirred for 1 h to obtain a homogenous solution. This solution was cast on to a poly propylene petri dish and was kept to dry at room temperature for few day to obtain the free standing nanocomposite film. Different Al₂O₃ concentrations PNC films were prepared simultaneously by following the same procedure. Finally, the PVA- x wt% Al₂O₃ films were dried in vacuum oven at 40 °C for 24 h to remove the water traces, if any, and after that these films were used for their structural and dielectric measurements.

Measurements

The X-ray diffraction (XRD) patterns of the Al₂O₃ nanopowder and PVA- x wt% Al₂O₃ films were recorded in reflection mode at a scan rate of 0.05 degree/s using a PANalytical X'pertPro MPD diffractometer of Cu-K α radiation (0.15418 nm wavelength). The X'pert pro® software was used for determination of angular position, intensity and full width at half maximum of the diffraction peaks in the XRD pattern.

The dielectric relaxation spectroscopic (DRS) measurements of the PNC films were carried out using an Agilent technologies 4284A precision LCR meter and 16451B solid dielectric test fixture in the frequency range of 20 Hz to 1 MHz at fixed temperature 30 °C. For PVA-3 wt% Al₂O₃ film the measurements were also carried out at temperatures 40, 50 and 60 °C. The frequency dependent values of capacitance C_p , resistance R_p and loss tangent ($\tan\delta = \epsilon''/\epsilon'$) in parallel mode operation of the dielectric test fixture loaded PNC film were measured. The spectra of intensive quantities, namely complex

dielectric function $\epsilon^*(\omega) = \epsilon' - j\epsilon''$, alternating current (ac) electrical conductivity $\sigma^*(\omega) = \sigma' + j\sigma''$ and electric modulus $M^*(\omega) = M' + jM''$, and the extensive quantity i.e. complex impedance $Z^*(\omega) = Z' - jZ''$ of the PNC films were determined using the C_p , R_p and $\tan\delta$ values in the equations described elsewhere [7]. These complex dielectric and electric functions can be transformed to each other according to the scheme $1/\epsilon^*(\omega) = j\omega C_0 Z^*(\omega) = M^*(\omega) = j\omega\epsilon_0/\sigma^*(\omega)$, where $\omega = 2\pi f$ is an angular frequency of the applied ac electric field, C_0 is the capacitance of the empty test fixture and ϵ_0 (8.85 pF/m) is the permittivity in vacuum.

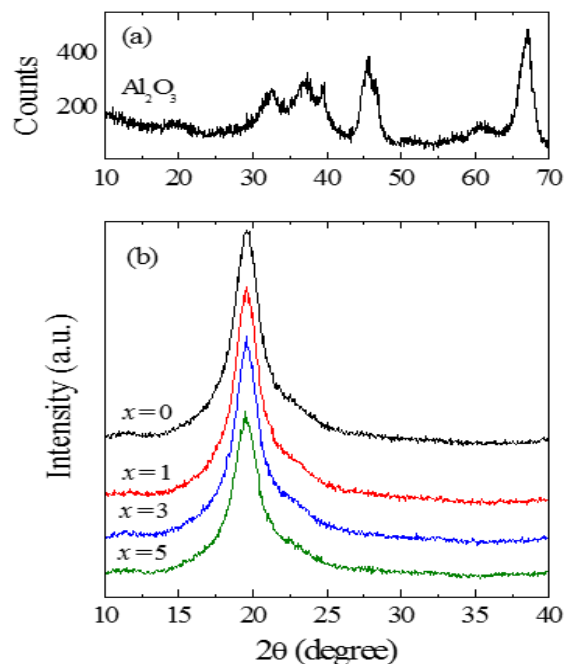


Fig. 1. XRD patterns of (a) γ -Al₂O₃ nanopowder and (b) PVA- x wt% Al₂O₃ nanocomposite films.

Results and discussion

XRD patterns and structural analysis

The XRD patterns of Al₂O₃ nanopowder and PVA- x wt% Al₂O₃ nanocomposite films are shown in **Fig. 1(a and b)**. The Al₂O₃ nanopowder used in the present study is of gamma phase because its diffraction peaks positions and their intensities (**Fig. 1a**) are in consistent with the literature values of γ -Al₂O₃[21–24]. The values of d -spacing corresponding to major crystalline peaks of γ -Al₂O₃ were determined by the Bragg's relation $\lambda = 2d\sin\theta$, where λ is the wavelength of X-ray radiation, d is the spacing between diffractive lattice planes (hkl) and θ is the measured diffraction angle (Bragg's angle) of the respective peaks. The values of crystallite sizes L were evaluated by Scherrer's equation $L = \lambda k/\beta\cos\theta$, where $k = 0.94$ is a constant and β is full width at half maximum (FWHM) (i.e. the broadening of peak at half-height expressed in radians of 2θ which is obtained by width measured in 2θ degrees and then multiplied by $\pi/180$). The values of 2θ , d , FWHM and L along with peak

intensities (counts) I of γ - Al_2O_3 nanoparticles are given in **Table 1**. The average crystallite size of γ - Al_2O_3 from its major crystalline peaks was found 5 nm, which is lower than its maximum particles size 50 nm. This finding shows that one grain in Al_2O_3 nanoparticles consists of approximately ten crystallites.

The broad and intense diffraction peak of pure PVA film at $2\theta = 19.59^\circ$ (**Fig. 1b**) confirms its semicrystalline structure as reported earlier [26,27]. This peak is corresponding to concurrent crystal reflections 101 and $10\bar{1}$ of the PVA. The crystallinity in pristine PVA network is developed due to intermolecular hydrogen-bonding between hydroxyl groups of the neighbouring PVA chains [27].

When 1, 3 and 5 wt% Al_2O_3 amounts are dispersed in PVA matrix, the PVA peak position remains unaltered but there is significant decrease in intensity of the peak with the increase of Al_2O_3 concentration (**Table 1**). The decrease of crystalline peak intensity of PVA with addition of Al_2O_3 reveals that there is formation of hydrogen bonds between $-\text{OH}$ groups of PVA with the oxygen atoms exist on the surface of Al_2O_3 nanoparticles, which confirm the surface passivation of PVA on Al_2O_3 nanoparticles. Due to PVA and Al_2O_3 interactions, the strength of intermolecular H-bonding between PVA chains reduces, and thereby leads to the decreasing amount of PVA crystallinity. This result is found in agreement with the PVA based solid polymer electrolyte in which the crystallinity of polymer decreases and simultaneously increases the ionic conductivity with the addition of Al_2O_3 nanofiller [28]. The d spacing and crystallite size L of PVA in the nanocomposites were determined by the Bragg's relation and the Scherrer's equation, respectively, and these are given in **Table 1**. The relative intensity RI values of the PVA peak in the nanocomposites were also determined with respect to peak intensity of pristine PVA. **Fig. 2** shows that the L and RI values of PVA- x wt% Al_2O_3 nanocomposites vary non-linearly with the increasing concentration of Al_2O_3 . It is found that for the investigated nanocomposites L increases whereas RI decreases with increase of Al_2O_3 concentration confirming the formation of bigger size crystallites with decrease of total crystalline phase of the PVA matrix.

Table 1. Values of Bragg's angle 2θ , basal spacing d , full width at half maximum FWHM, crystallite size L , peak intensity (counts) I and relative intensity RI of Al_2O_3 nanopowder and PVA- x wt% Al_2O_3 nanocomposite films.

Al_2O_3	2θ	d	FWHM	L	I	
(degree)	(nm)	$\times 10^3$ (rad)	(nm)	(counts)		
	45.51	0.199	40.58	3.87	263	
	67.07	0.139	31.29	5.55	375	
PVA- x wt% Al_2O_3	2θ	d	FWHM	L	I	RI
x	(degree)	(nm)	$\times 10^3$ (rad)	(nm)	(counts)	(%)
0	19.59	0.4528	34.75	4.23	2969	100
1	19.58	0.4530	33.42	4.40	2935	98.9
3	19.58	0.4530	32.76	4.49	2702	91.0
5	19.54	0.4539	32.17	4.57	2113	71.2

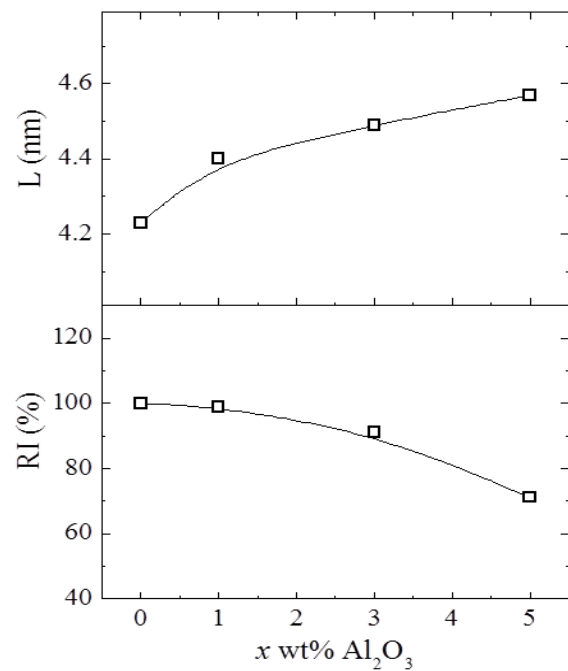


Fig. 2. Al_2O_3 concentration dependent crystallite size L and relative intensity RI of PVA- x wt% Al_2O_3 nanocomposite films.

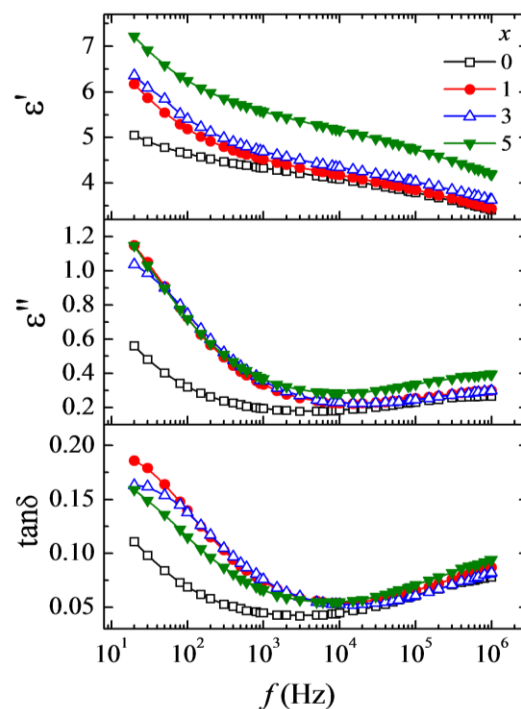


Fig. 3. Frequency dependent real part ϵ' and loss part ϵ'' of the complex dielectric function, and loss tangent $\tan\delta$ of PVA- x wt% Al_2O_3 nanocomposite films at 30°C .

Al_2O_3 concentration dependent dielectric behaviour of PNC films

Frequency dependent real part ϵ' and loss part ϵ'' of complex dielectric function (permittivity) and loss tangent (dissipation factor) $\tan\delta = \epsilon''/\epsilon'$ spectra of PVA- x wt% Al_2O_3 nanocomposites at 30°C are shown in **Fig. 3**. The ϵ' values of these PNC films non-linearly decrease with

increase of frequency which is due to the fact that at low frequency the orientation of electric dipoles of PVA chains follows the varying electric field but as the frequency increases they can no longer follow the fast field changes. Further, large increase of ϵ' values of PNC films at low frequencies can be attributed to the interfacial polarization which exists due to the difference in the permittivity values of the Al_2O_3 and PVA matrix. The contribution of interfacial polarization in enhancement of dielectric permittivity, particularly in the low frequency region, is a common phenomenon in PNC materials [7–10, 29–31]. Fig. 3 shows that the shape of ϵ'' and $\tan\delta$ spectra of the nanocomposites are nearly identical and these spectra have minimum values in the intermediate frequency region. The increasing tendency of ϵ'' and $\tan\delta$ values in the high frequency and low frequency regions of these spectra infers that there may be relaxation peaks beyond the experimental frequency range used in this study.

The Al_2O_3 concentration dependent ϵ' values of PNC films at fixed frequencies are shown in Fig. 4. The dielectric permittivity of Al_2O_3 is 9.7 at 1 MHz [16] which is nearly three times high as compared to that of the pristine PVA, and therefore, the ϵ' values of the nanocomposites should increase with the increase of Al_2O_3 concentration as per composition additive relation of the complex dielectric. For polymer-alumina nanocomposites, the mechanism involved in enhancement of the dielectric properties with increase of alumina concentration is also established by performing *ab initio* molecular orbital calculations [32]. According to this calculation the strong electrostatic attraction between alumina and polymer results in an increase in the dipole moment and the polarization of the composite system leading to enhanced dielectric properties. Fig. 4 clearly shows that the ϵ' values non-linearly increase with the increase of Al_2O_3 concentration in the nanocomposites. Further, the increase of ϵ' is found high at low frequency (e.g. 100 Hz) as compared to that of the high frequency (e.g. 1 MHz) for these nanocomposites. These results suggest that the ϵ' values of these polymeric nanocomposites can be tuned to the desired values at a particular frequency by adjusting the loaded Al_2O_3 concentration in the PVA matrix.

Electric modulus spectra

The complex electric modulus spectra ($M^*(\omega) = 1/\epsilon^*(\omega)$) of the PNC materials are shown in Fig. 5. These spectra are mostly studied for confirmation of bulk response of the material i.e. without any contribution of electrode polarization effect [7–10]. It is found that M' values non-linearly increase with increase of frequency, whereas M'' spectra of these materials (1 and 3 wt% Al_2O_3) exhibit a relaxation process peak near low frequency end of the spectra which may be assigned to the PVA local chain motion. From these spectra, it can be suggested that the PVA chain segmental dynamics is influenced by the concentration of Al_2O_3 nanofiller.

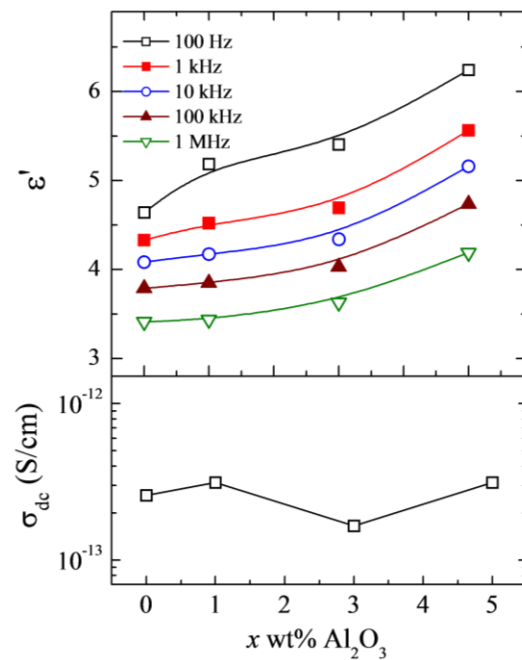


Fig. 4. Al_2O_3 concentration dependent ϵ' and dc conductivity σ_{dc} values of PVA- x wt% Al_2O_3 nanocomposite films at 30 °C.

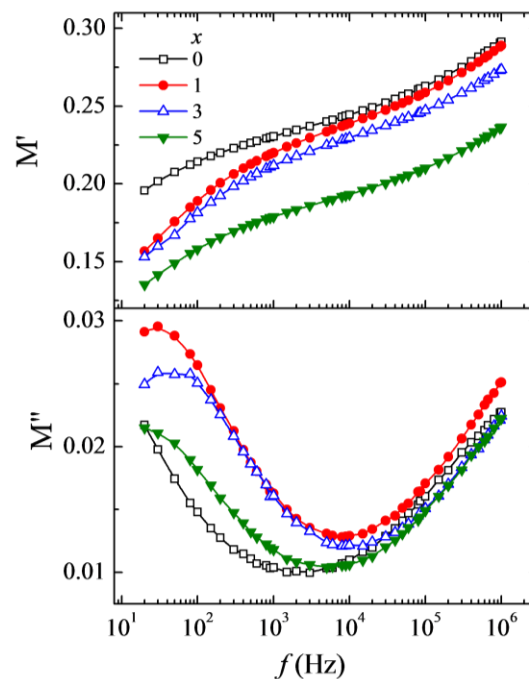


Fig. 5. Frequency dependent real part M' and loss part M'' of complex electric modulus of PVA- x wt% Al_2O_3 nanocomposite films at 30 °C.

AC conductivity and impedance spectra

The spectra of real part σ' and loss part σ'' of the complex ac electrical conductivity of PVA- x wt% Al_2O_3 nanocomposites at 30 °C are shown in upper layer of Fig. 6. It is found that the σ' values vary linearly in low frequency region and also in high frequency region with different values of their slopes. Further, the σ'' values over the entire frequency range increase linearly with the

increase of frequency. At low frequencies, long-range transport of charges occurs through the semiconducting islands in the insulating PVA matrix, and therefore, the rate of increase of σ' is low but as the frequency increases the localized charge carrier contribution increases and hence the ac conductivity also increases linearly for these materials. Further the frequency dependent σ' values are found lower than that of the corresponding σ'' values of the investigated PNC materials. The σ' values of these nanocomposites are lower than 10^{-10} S/cm at 20 Hz, and with the increase of frequency it attains the value higher than 10^{-7} S/cm at 1 MHz. The σ_{dc} values of these nanocomposite films were estimated by interpolation of the σ' spectra up to $f \rightarrow 0$. The observed σ_{dc} values of the PNC films are plotted in Fig. 4 which vary anomalously with increase of Al_2O_3 concentration in the nanocomposites.

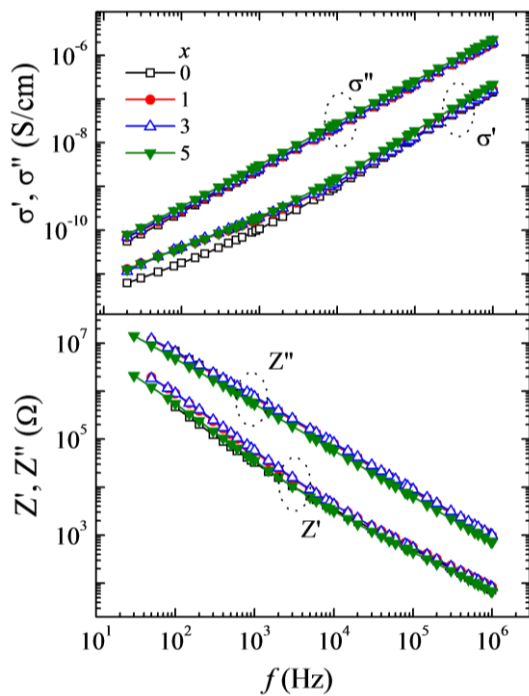


Fig. 6. Frequency dependent real part σ' and loss part σ'' of the complex ac electrical conductivity, and real part Z' and reactive part Z'' of complex impedance of PVA- x wt% Al_2O_3 nanocomposite films at 30 °C.

The impedance spectra (real part Z' and reactive part Z'') of the PVA- x wt% Al_2O_3 films, at 30 °C, are depicted in lower layer of Fig. 6. It is observed that both the Z' and Z'' values of the nanocomposites decrease with the increase of frequency and have small variation with change of filler concentrations. The Z'' values are found high as compared to the Z' values at same frequency which suggest the dominant capacitive behaviour of these materials. Further, the low frequency impedance values of these materials are of several M Ω which confirm their good electrical insulation behaviour at low frequencies, and therefore these materials can be recognized as nanodielectric insulators for audio frequencies operated microelectronic devices.

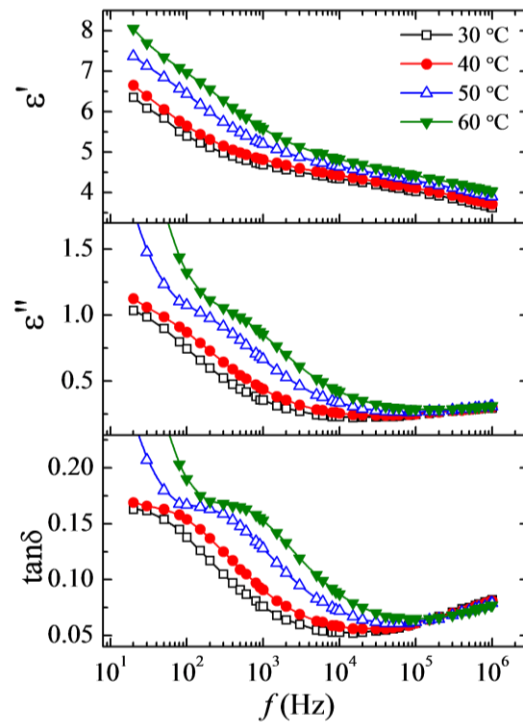


Fig. 7. Frequency dependent real part ϵ' and loss ϵ'' of the complex dielectric function, and loss tangent $\tan\delta$ of PVA-3 wt% Al_2O_3 nanocomposite film at different temperatures.

Effect of temperature on dielectric behaviour of PNC film

The ϵ' , ϵ'' and $\tan\delta$ spectra of PVA-3 wt% Al_2O_3 nanocomposite film at different temperatures are shown in Fig. 7. It is observed that the ϵ' spectra have uniform enhancement with the increase of temperature. In order to confirm the behaviour of ϵ' values with temperature at fixed frequencies, these ϵ' values are plotted against temperature in Fig. 8. It is observed that the ϵ' values of the nanocomposite increase linearly with increase of temperature at radio frequencies but this increase is non-linear at audio frequencies of the exciting electric field.

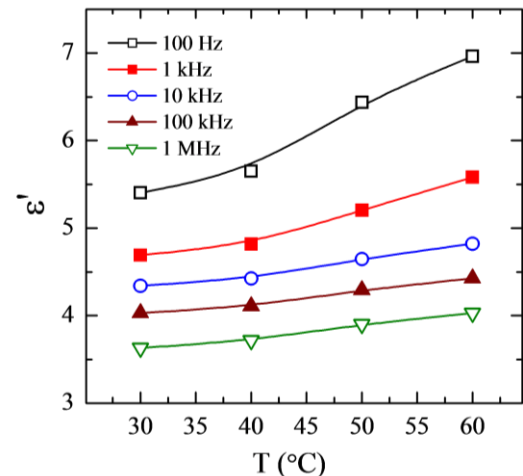


Fig. 8. Temperature dependent ϵ' values of PVA-3 wt% Al_2O_3 nanocomposite film.

The interfacial polarization effect and dc conductivity contribution at low frequencies are the reasons behind the strong increase of ϵ' values from linearity with increase of temperature of the studied PNC film. The inflexion in ϵ'' spectra and the appearance of relaxation peaks in $\tan\delta$ spectra at lower frequencies clearly reveal that the low frequency relaxation process is due to PVA local chain motion, and this process shifts to higher frequency side with increasing temperature (Fig. 7). Since, thermal agitation increases the free volume, and hence facilitates the orientation of dipolar segments of thermally activated PVA chain in the nanocomposite resulting in decrease of relaxation time.

The M' and M'' spectra of PVA-3 wt% Al_2O_3 film at different temperatures are shown in Fig. 9. The M'' spectra exhibit a PVA chain segmental motion relaxation peak in lower frequency region, at all the temperatures which shift towards higher frequency side with a small increase of its magnitude as the temperature of PNC film increases. The relaxation time τ of the PNC film is determined using the frequency f_p value corresponding to the M'' peak from the relation $\tau = (2\pi f_p)^{-1}$, which is found of the order of millisecond.

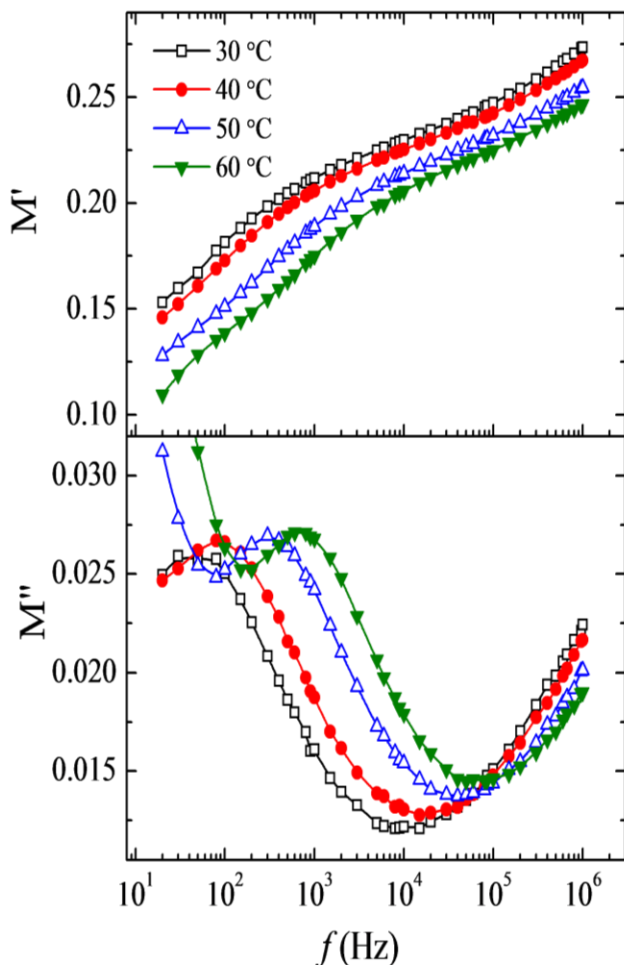


Fig. 9. Frequency dependent real part M' and loss part M'' of complex electric modulus of PVA-3 wt% Al_2O_3 nanocomposite film at different temperatures.

The σ' and σ'' spectra of PVA-3 wt% Al_2O_3 nanocomposite film at different temperatures are depicted in Fig. 10. It can be seen from the figure that there is a small increase of σ' with increase of temperature of the film confirming its semiconducting-type behaviour. The σ'' values of PNC film increase linearly with increase of frequency, at constant temperature, and also increase with the increase of temperature at fixed frequency, as shown in enlarged view of the figure. The temperature dependent dc conductivity σ_{dc} values of the PNC film were estimated by interpolation of low frequencies $\sigma'(T)$ spectra up to dc field.

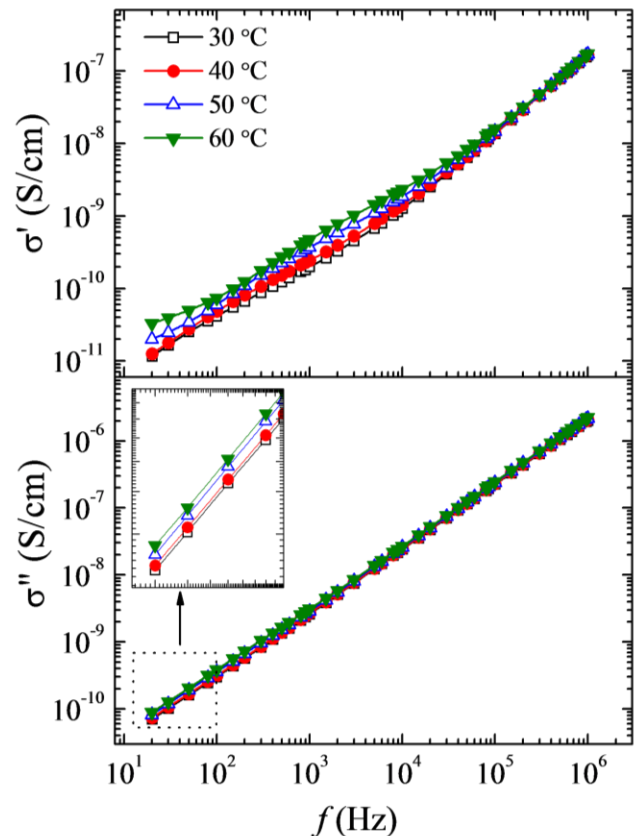


Fig. 10. Frequency dependent real part σ' and loss part σ'' of the complex ac electrical conductivity of PVA-3 wt% Al_2O_3 nanocomposite film at different temperatures. Inset shows the enlarged view of σ'' values at low frequencies.

The temperature dependent observed τ and σ_{dc} values of PVA-3 wt% Al_2O_3 film are plotted against $1000/T$ in Fig. 11. The linear variation of these plots confirms their Arrhenius behaviour. Therefore, the relaxation time and conductivity activation energies E_τ and E_σ of the PVA-3 wt% Al_2O_3 film are determined using the Arrhenius relations $\tau = \tau_0 \exp(E_\tau/kT)$ and $\sigma_{dc} = \sigma_0 \exp(-E_\sigma/kT)$, respectively. The E_τ and E_σ values of the PNC film as marked in the figure are found 0.83 eV and 1.02 eV, respectively, which reveals that the PVA segmental dynamics have relatively low barrier as compared to the barrier height for charge transportation in the studied PNC film.

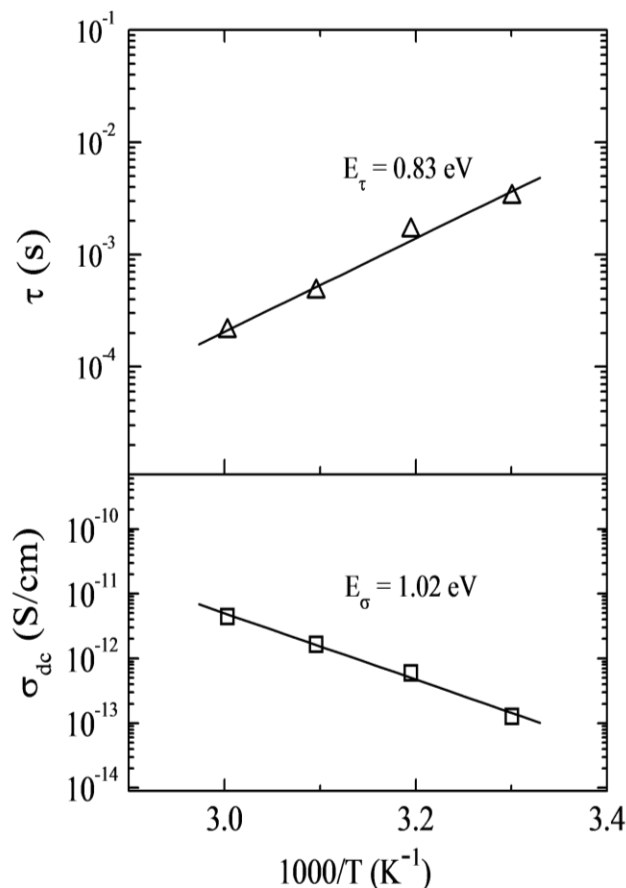


Fig. 11. Arrhenius behaviour of relaxation time τ and dc conductivity σ_{dc} of PVA-3 wt% Al_2O_3 nanocomposite film.

Conclusion

The dielectric and electrical properties of PVA- x wt% Al_2O_3 nanocomposites are reported. The real part of permittivity non-linearly increases with the increase of Al_2O_3 concentration in the nanocomposites. The temperature dependent ϵ' values exhibit linear behaviour at high frequencies and non-linear behaviour at low frequencies of the excitation electric field. The structural relaxation time and dc conductivity of PVA-3 wt% Al_2O_3 nanocomposite obey the Arrhenius behaviour. Due to PVA and Al_2O_3 interactions the crystalline phase of PVA decreases with increase of Al_2O_3 concentration in these nanocomposite materials. The frequency and temperature dependent dielectric permittivity and electrical conductivity values of these materials confirm their suitability as flexible-type nanodielectric materials for their use as insulator and substrate in design of microelectronics devices.

Acknowledgements

Authors are grateful to the Department of Science and Technology (DST), New Delhi for providing the experimental facilities through research projects Nos. SR/S2/CMP-09/2002, SR/S2/CMP-0072/2010 and the DST-FIST program. One of the authors SC is thankful to the DST, New Delhi for the award of

SERB Fast Track Young Scientist research project No. SR/FTP/PS-013/2012.

References

- Tan, D.; Irwin, P.; Polymer Based Nanodielectric Composites, In Advances in Ceramics, Sikalidis, C. (Ed.); InTech: Croatia, **2011**. DOI: 10.5772/23012
- Keith, N. J.; Dielectric Polymer Nanocomposites; Springer Science + Business Media, LLC, **2010**. DOI: 10.1007/978-1-4419-1591-7
- Reddy, B. S. R.; Advances in Nanocomposites - Synthesis, Characterization and Industrial Applications; InTech: Croatia, **2011**.
- Mittal, V.; Characterization Techniques for Polymer Nanocomposites; Wiley-VCH Verlag GmbH & Co. KgaA, **2012**. DOI: 10.1002/9783527654505
- Sugumar, S.; Bellan, C. S.; *Optik*, **2014**,125, 5128. DOI: 10.1016/j.ijleo.2014.04.077
- Kinadjian, N.; Achard, M. F.; López, B. J.; Maugey, M.; Poulin, P.; Prouzet, E.; Backov, R.; *Adv. Funct. Mater.*, **2012**,22, 3994. DOI: 10.1002/adfm.201200360
- Sengwa, R. J.; Choudhary, S.; Sankhla, S.; *Compos. Sci. Technol.*, **2010**,70, 1621. DOI: 10.1016/j.compscitech.2010.06.003
- Choudhary, S.; Sengwa, R. J.; *J. Appl. Polym. Sci.*, **2012**,124, 4847. DOI: 10.1002/app.35556
- Choudhary, S.; Sengwa, R. J.; *Polym. Bull.*, **2015**,72, 2591. DOI: 10.1007/s00289-015-1424-2
- Sinha, S.; Chatterjee, S. K.; Ghosh, J.; Meikap, A. K.; *Polym. Compos.*, **2017**,38, 287. DOI: 10.1002/pc.23586
- Sugumar, S.; Bellan, C. S.; Muthu, D.; Raja, S.; Bheeman, D.; Rajamani, R.; *Polym. Adv. Technol.*, **2015**,26, 1486. DOI: 10.1002/pat.3568
- Chibowski, S.; Paszkiewicz, M.; Krupa, M.; *Powder Tech.*, **2000**,107, 251.
- Sonmez, M.; Fica, D.; Stan, A.; Bleotu, C.; Matei, L.; Fica, A.; Andronescu, E.; *Mater. Lett.*, **2012**,74, 132. DOI: 10.1016/j.matlet.2012.01.062
- Lamastra, F. R.; Bianco, A.; Meriggi, A.; Montesperelli, G.; Nanni, F.; Gusmano, G.; *Chem. Eng. J.*, **2008**,145, 169. DOI: 10.1016/j.cej.2008.07.048
- Mallakpour, S.; Sirous, F.; *Prog. Org. Coatings*, **2015**,85, 138. DOI: 10.1016/j.porgcoat.2015.03.021
- Mallakpour, S.; Khadem, E.; *Prog. Polym. Sci.*, **2015**,51, 74. DOI: 10.1016/j.progpolymsci.2015.07.004
- Mallakpour, S.; Dinari, M.; *J. Reinf. Plast. Compos.*, **2013**, 32, 217. DOI: 10.1177/0731684412467236
- Nigralaw, A.; Chand, N.; *Prog. Nanotech. Nanomater.*, **2013**,2, 25.
- Sugumar, S.; Bellan, C. S.; Nadimuthu, M.; *Iranian Polym. J.*, **2015**,24, 63. DOI:10.1007/s13726-014-0300-5
- Evan, K. A.; *Key Eng. Mater.*, **1996**,122-124, 489.
- Tok, A. I. Y.; Boey, F.Y.C.; Zhao, X. L.; *J. Mater. Proc. Tech.*, **2006**,178, 270. DOI: 10.1016/j.jmatproctec.2006.04.007
- Santos, P. S.; Santos, H. S.; Toledo, S. P.; *Mater. Res.*, **2000**,3, 104.
- Jian-hong, Y. I.; You-yi, S.; Jian-feng, G. A. O.; Chun-yan, X. U.; *Trans. Nanoferrous Met. Soc. China*, **2009**,19, 1237. DOI: 10.1016/S1003.6326(08)60435-5
- Wang, Y.; Shih, K.; Jiang, X.; *Ceram. Int.*, **2012**,38, 1879. DOI: 10.1016/j.ceramint.2011.10.015
- Khom, J.; Prasertdam, P.; Panpranot, J.; Mekasuwandumrong, O.; *Catalysis Comm.*, **2008**,9, 1955. DOI: 10.1016/j.catcom.2008.03.009
- Choudhary, S.; Sengwa, R. J.; *J. Appl. Polym. Sci.*, **2014**,131, 40617. DOI: 10.1002/app.40617
- Rao, J. K.; Raizada, A.; Ganguly, D.; Mankad, M. M.; Satayanarayana, S. V.; Madhu, G. M.; *J. Mater. Sci.*, **2015**,50, 7064. DOI: 10.1007/s10853-015-9261-0
- Mohamad, A. A.; Arof, A. K.; *Mater. Lett.*, **2007**,61, 3096. DOI: 10.1016/j.matlet.2006.11.030

29. Choudhary, S.; Sengwa, R. J.; *Express Polym. Lett.*, **2010**,9, 559.
DOI: 10.3144/expresspolymlett.2010.70
30. Sengwa, R. J.; Choudhary, S.; *Macromol. Symp.*, **2016**, 362, 132.
DOI: 10.1002/masy.201400259
31. Tuncer, E.; Rondinone, A. J.; Woodward, J.; Sauers, I.; James, D. R.; Ellis, A. R.; *Appl. Phys. A*, **2009**, 94, 843.
DOI: 10.1007/s00339-008-4881-8
32. Jacob, R.; Jacob, A. P.; Mainwaring, D. E.; *J. Mol. Struct.*, **2009**,933, 77.
DOI:10.1016/j. molstruc.2007.05.041